

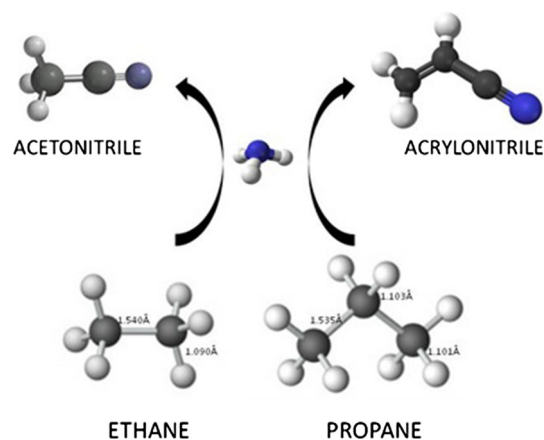
# Propane Versus Ethane Ammoxidation on Mixed Oxide Catalytic Systems: Influence of the Alkane Structure

M. Olga Guerrero-Pérez<sup>1</sup> · Elizabeth Rojas-García<sup>2,3</sup> · Ricardo López-Medina<sup>2,3</sup> · Miguel A. Bañares<sup>3</sup>

Received: 15 March 2016 / Accepted: 7 July 2016 / Published online: 23 July 2016  
© Springer Science+Business Media New York 2016

**Abstract** Catalysts from three different catalytic systems, Ni–Nb–O, Mo–V–Nb–Te–O and Sb–V–O, have been prepared, characterized, and tested during both ethane and propane ammoxidation reactions, in order to obtain acetonitrile and acrylonitrile, respectively. The catalytic results show that Mo–V–Nb–Te–O and Sb–V–O catalyze propane ammoxidation but are inactive for ethane ammoxidation whereas Ni–Nb–O catalysts catalyze both, ethane and propane ammoxidation. The activity results, and the characterization of fresh and used catalysts along with some data from previous studies, indicate that the ammoxidation reaction mechanism that occurs in these catalytic systems is different. In the case of Mo–V–Nb–Te–O and Sb–V–O, two active sites appear to be involved. In the case of Ni–Nb–O catalysts, only one site seems to be involved, which underlines that the mechanism is different and take place via a different intermediate. These catalysts activate the methyl groups in ethane, on the contrary, neither ethane nor ethylene appear to adsorb on the Mo–V–Nb–Te–O and Sb–V–O active sites.

## Graphical Abstract



**Keywords** Ethane · Propane · Ammoxidation · NiO · SbVO<sub>4</sub> · Multioxide catalysts

## 1 Introduction

Ammoxidation reactions refer to the oxidation using molecular oxygen in the presence of ammonia. They are generally used for the synthesis of nitrile-based compounds (R–CN). The ammoxidation of several hydrocarbons to prepare a wide range of commercially important nitriles has been the subject of great interest in recent years because nitriles are very useful basic molecules or organic intermediates (e.g. nicotinonitrile) used in the manufacture of numerous value-added chemicals [1]. Light alkanes, such as ethane and propane, can also undergo ammoxidation, and these reactions are receiving an increasing interest nowadays due to the increasing relevance of shale gas,

✉ M. Olga Guerrero-Pérez  
oguerro@uma.es

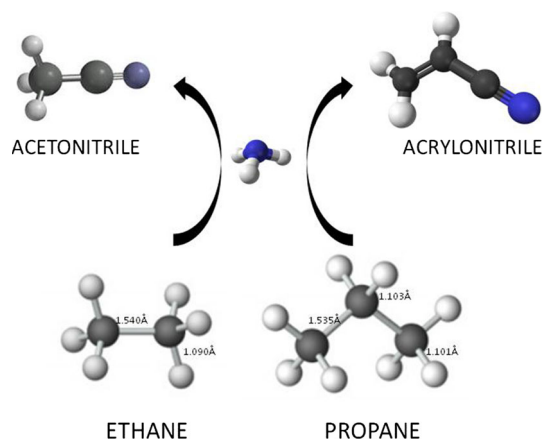
<sup>1</sup> Departamento de Ingeniería Química, Andalucía Tech, Universidad de Málaga, 29071 Málaga, Spain

<sup>2</sup> Departamento de Ciencias Básicas, Universidad Autónoma Metropolitana-Azcapotzalco, Av. San Pablo 180, Col. Reynosa Tamaulipas, Ciudad de México 02200, Mexico

<sup>3</sup> SpeiCat, Spectroscopy and Industrial Catalysis, Instituto de Catálisis y Petroleoquímica; ICP-CSIC, Marie Curie 2, 29049 Madrid, Spain

mainly in northern America; such interest is spreading to the rest of the world. Acrylonitrile is a valuable chemical that can be synthesized through propane ammoxidation. It is widely used as an intermediate for the preparation of synthetic rubbers, synthetic resins and carbon and acrylic fibers. It is a very common monomer to prepare several polymers: such as polyacrylonitrile, styrene-acrylonitrile (SAN), acrylonitrile butadiene styrene (ABS), acrylonitrile styrene acrylate (ASA) or acrylonitrile butadiene (NBR) [2]. Propane ammoxidation is now available at a commercial scale, since very recently Asahi Kasei Chemical opened a plant in Thailand for a propane ammoxidation process [3]. It is expected that propane-based technology will replace the propylene-based technology within the next years. The ammoxidation of ethane produces acetonitrile. It is used as a solvent in many commercial processes, such as high performance liquid chromatography or for the butadiene extraction in hydrocarbon streams. It is also used in several organic and inorganic syntheses, such as the synthesis of flavones and flavonol pigments. Currently, acetonitrile is obtained as a by-product during the propylene ammoxidation since there is no method for the direct commercial synthesis of acetonitrile. Thus both reactions, ammoxidation of propane or ethane in the presence of oxygen and ammonia to obtain the corresponding nitrile, are of interest nowadays. These reactions share similarities that result in different catalyst requirements. The key difference is that all C–H bonds in ethane are equivalent and primary, whereas propane also has a secondary carbon –CH<sub>2</sub>–, a methylene group. Thus, the activation of ethane and propane is not equivalent (Scheme 1)

The objective of this work is to analyze the catalytic behavior of different mixed oxide catalytic systems during both ethane and propane ammoxidation reactions in order to have an insight into the similarities and differences on both reaction mechanisms and also to have a deeper



**Scheme 1** Scheme of reactions studied (bond lengths of in propane and ethane molecules are indicated)

knowledge on the active sites of these catalytic systems. To achieve these objectives, three catalytic systems will be prepared and characterized: Ni–Nb–O, Sb–V–O and Mo–V–Nb–Te–O.

It was reported by Lemonidou and co-workers that Nb-promoted NiO catalysts activate ethane for its oxidative dehydrogenation [4, 5]. After that, our group reported that Ni–Nb–O oxide catalysts are also promising during the direct ammoxidation of ethane to acetonitrile [6, 7]. These results have shown how the incorporation of a small amount of niobium into the NiO lattice induces an enhancement of the activity of these catalysts during the ammoxidation of ethane into acetonitrile [8]. Two different mixed Nb–Ni–O phases were identified, with different Nb/Ni atomic ratios. A Nb-poor Nb–Ni–O phase with a particle size in the 20–50 nm range; and a Nb-rich Nb–Ni–O phase that presents a smaller particle size [9, 10].

Sb–V–O based catalysts are active and selective for several partial oxidation reactions [11–13]. They exhibit good performances for some processes such as the transformation of H<sub>2</sub>S to elemental sulphur [14], the methane oxidation to formaldehyde [15], the destruction of nitrogen-containing organic molecules [16], or the oxidation of isobutene into methacrolein [17]. But the process for which they have been most studied, is for the ammoxidation of propane [18–20], and, recently, it has been reported also the ammoxidation of glycerol over this catalytic system [21–23]. VSbO<sub>4</sub> rutile phase is the main active phase of this catalytic system, due to its redox behaviour [24–30].

Mo–V–Te–(Nb)–O multioxide mixed metal catalysts have been described as selective for the ammoxidation of propane to acrylonitrile by several authors [31–41]. These Mo–V oxide based catalytic materials present several active phases, denoted as M1, M2 and rutile [42]. The M1 phase [(TeO)<sub>1-x</sub>M<sub>10</sub>O<sub>28</sub> orthorhombic] crystallizes in the orthorhombic system and undergoes oxidation and reduction to a certain degree without significant structural changes [43–47]. The M2 phase (Te<sub>0.33</sub>MO<sub>3.33</sub> pseudo-hexagonal) crystallizes in the orthorhombic system [48]. It seems that there is a synergistic effect between these two phases; M1 is described as a phase able to activate the propane molecule, whereas M2 would improve the selectivity of the catalysts towards acrylic acid formation [10, 49, 50]. The data of these active phases have been reported before. M1 (Mo<sub>7.8</sub>V<sub>1.2</sub>NbTe<sub>0.94</sub>O<sub>28.9</sub>) and M2 (Mo<sub>4.31</sub>V<sub>1.36</sub>Te<sub>1.81</sub>Nb<sub>0.33</sub>O<sub>19.81</sub>); M1 (Pba2 unit cell, with a = 21.134 Å, b = 26.658 Å, c = 4.0146 Å and Z = 4) and M2 (Pmm2 unit cell, with a = 12.6294 Å, b = 7.29156 Å, c = 4.02010 Å and Z = 4) [51]. VSbO<sub>4</sub> lattice parameters have been reported [52] and the sizes of the unit cell are similar, with a = b = 4.636 Å and c = 9.114 Å. NiO

crystallizes in the cubic rock salt structure, with a lattice parameter of  $a = 4.1694 \text{ \AA}$ .

## 2 Experimental Section

The synthesis procedure for the Ni–Nb mixed oxide catalysts has been reported in detail previously [8]. Ammonium niobium soluble complex (niobium products) was added to an aqueous solution nickel acetate tetrahydrate (>99 %, Aldrich), this solution was kept under stirring at 80 °C during 1 h to ensure complete dissolution and good mixing of the starting compounds. The resulting solution was dried in a rotary evaporator at 80 °C at reduced pressure of 10–40 mmHg. The resulting solid was dried at 120 °C for 24 h and then heated in air at a rate of 5 °C min<sup>-1</sup> to 450 °C and held during 5 h. The nomenclature of catalysts was as follows: Ni<sub>y</sub>Nb<sub>x</sub>-O, where y and x indicate the atomic content of Ni and Nb, respectively.

The Sb–V–O catalytic system was prepared as a supported phase. This facilitates obtaining the active phase and characterizing the surface species [53, 54]. The Sb–V–O supported catalyst was prepared by dissolving the required amount of antimony acetate (Aldrich) in tartaric acid (Sigma) 0.3 M. This solution was kept under stirring until all antimony dissolves. Then, NH<sub>4</sub>VO<sub>3</sub> (Sigma) and the  $\gamma$ -Al<sub>2</sub>O<sub>3</sub> (Sasol, Puralox SCCa-5/200) support were added. The solution was dried in a rotatory evaporator at 80 °C and 0.3 atm. The resulting solid was dried at 115 °C for 24 h and then calcined at 400 °C for 4 h in air. The catalyst was prepared so that a total coverage of V+Sb of 12 atoms per nm<sup>2</sup> of alumina support and Sb/V molar ratio of 1 has been selected as optimum for the formation of small aggregates of the active phase (VSbO<sub>4</sub>) on the surface of catalysts.

Supported catalysts were prepared for the study with the multioxide system. The catalysts named as Mo<sub>5</sub>V<sub>4</sub>Nb<sub>0.5</sub>Te<sub>0.5</sub>O-N (nitrogen) and Mo<sub>6</sub>V<sub>3</sub>Nb<sub>0.5</sub>Te<sub>0.5</sub>O-A (air) with a final Mo/V/Te/Nb atomic ratio of 0.5-0.6/0.4-0.3/0.05/0.05 were prepared from aqueous slurries of the corresponding salts, as reported elsewhere, and treated at 600 °C for 2 h in N<sub>2</sub> and air flow [55]. They were prepared in order to have a total Mo+V+Nb+Te coverage of 12 atoms per nm<sup>2</sup> on alumina support.

Nitrogen adsorption isotherms were recorded on an automatic Micromeritics ASAP-2000 apparatus. Prior to the adsorption experiments, samples were outgassed at 140 °C for 2 h. BET areas were computed from the adsorption isotherms ( $0.05 < P/P_0 < 0.27$ ), taking a value of 0.164 nm<sup>2</sup> for the cross-section of the adsorbed N<sub>2</sub> molecule at -196 °C. The catalysts were analyzed by XRD in a Siemens Krystalloflex D-500 diffractometer, with CuK $\alpha$  radiation, at  $\lambda = 1.5418 \text{ \AA}$  and a graphite

monochromator. Working conditions were 40 kV, 30 mA, and scanning rate of 2° min<sup>-1</sup> for Bragg's angles 2 $\theta$  from 10 to 70°.

Activity measurements were performed using a conventional micro-reactor designed with minimized void volume. The feed stream and effluents of the reactor were analyzed by an online gas chromatograph equipped with a flame ionization and thermal-conductivity detectors. The correctness of the analytical determinations was checked for each test by verification that the carbon balance (based on the propane converted) was within the cumulative mean error of the determinations ( $\pm 10 \%$ ). The catalytic tests were made using 0.2 g of powder sample with particle dimensions in the 0.25–0.125 mm range. The axial temperature profile was monitored by a thermocouple sliding inside a quartz tube inserted into the catalytic bed. The catalysts were pre-treated in flowing air at 450 °C for 30 min. The reaction mixture feed was alkane/O<sub>2</sub>/NH<sub>3</sub>/He = 9.8/25/8.6/56.6. The total flow rate was 20 ml min<sup>-1</sup>, corresponding to 3000 h<sup>-1</sup> gas hourly-space velocity (GHSV). The quantity of catalyst and total flow were determined in order to avoid internal and external diffusion limitations. Yields and selectivities in products were determined on the basis of the moles of alkane feed and products, considering the number of carbon atoms in each molecule.

## 3 Results

The BET area values obtained for all the samples (bulk Ni–Nb–O, and alumina supported Sb–V–O and Mo–V–Nb–Te samples) are shown in Table 1; these range 45–155 m<sup>2</sup> g<sup>-1</sup>. Ni–Nb–O catalysts have a rather high surface area despite being unsupported; this should be due to the incorporation of Nb into the NiO lattice, which increases the surface area with respect pure NiO, reaching a maximum for the composition Ni<sub>0.6</sub>Nb<sub>0.4</sub>, as has been

**Table 1** BET surface area values of catalysts

Catalysts	BET area (m <sup>2</sup> g <sup>-1</sup> )
1.5Sb <sub>1</sub> V/Al	151
Ni <sub>0.9</sub> Nb <sub>0.1</sub>	57
Ni <sub>0.6</sub> Nb <sub>0.4</sub>	97
Ni <sub>0.35</sub> Nb <sub>0.65</sub>	84
Ni <sub>0.2</sub> Nb <sub>0.8</sub>	46
Mo <sub>5</sub> V <sub>4</sub> Nb <sub>0.5</sub> Te <sub>0.5</sub> O-N	123
Mo <sub>5</sub> V <sub>4</sub> Nb <sub>0.5</sub> Te <sub>0.5</sub> O-A	74
Mo <sub>6</sub> V <sub>3</sub> Nb <sub>0.5</sub> Te <sub>0.5</sub> O-N	125
Mo <sub>6</sub> V <sub>3</sub> Nb <sub>0.5</sub> Te <sub>0.5</sub> O-A	82

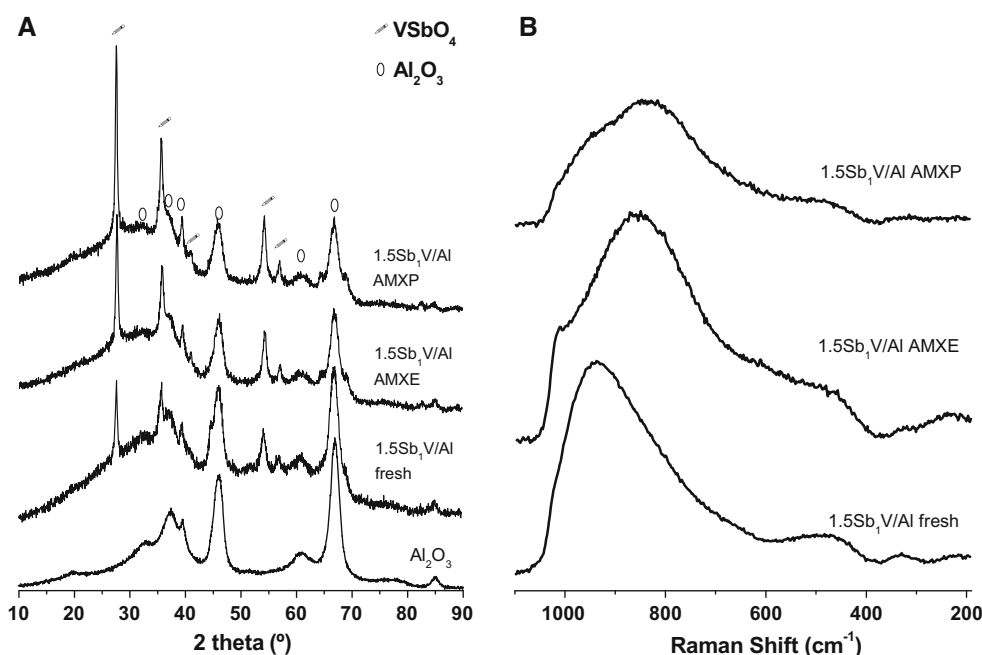
described elsewhere (9). The BET area values for Mo–V–Nb–Te treated under inert atmosphere present rather low areas. This fact has been described before for catalysts with similar formulation [56]. Since for these samples the coverage is up to 200 % monolayer coverage (ca. 12 atoms  $\text{n}^{-1}\text{m}^{-2}$ ), this may indicate that a layer of porous oxide structure develops over the catalytic support, and subsequently, those samples present higher surface area values [57].

Figure 1a shows the XRD patterns of fresh and used 1.5Sb1 V/Al catalyst after both propane and ethane ammoxidation reactions. Figure 1b shows the Raman spectra of the same samples. The XRD pattern of rutile  $\text{SbVO}_4$  is visible in the fresh sample and it grows stronger after use in reaction; this is indicative that antimony and vanadium oxide further blend during ammoxidation. Raman spectra (Fig. 1b) confirm these changes, which are in line with previous *operando* Raman studies [24, 26, 30]. Fresh catalyst presents a broad Raman band near  $900\text{ cm}^{-1}$ , typical of the V–O–V stretching mode of surface molecularly dispersed vanadium oxide species [58]. Antimony oxide is not detected by XRD, indicative that it must be dispersed. The Raman section of dispersed antimony oxide is extremely low, so it cannot be detected by Raman in the presence of species producing Raman bands [59]. Conversely crystalline antimony oxide phases ( $\text{Sb}_2\text{O}_3$ ,  $\text{Sb}_2\text{O}_4$ ) give rise to strong Raman bands [19]. Thus, Sb and V oxides appear highly dispersed on the surface of the fresh alumina-supported catalyst; this was expected since antimony was incorporated as soluble tartrate complex [59]. After ammoxidation reaction, a new

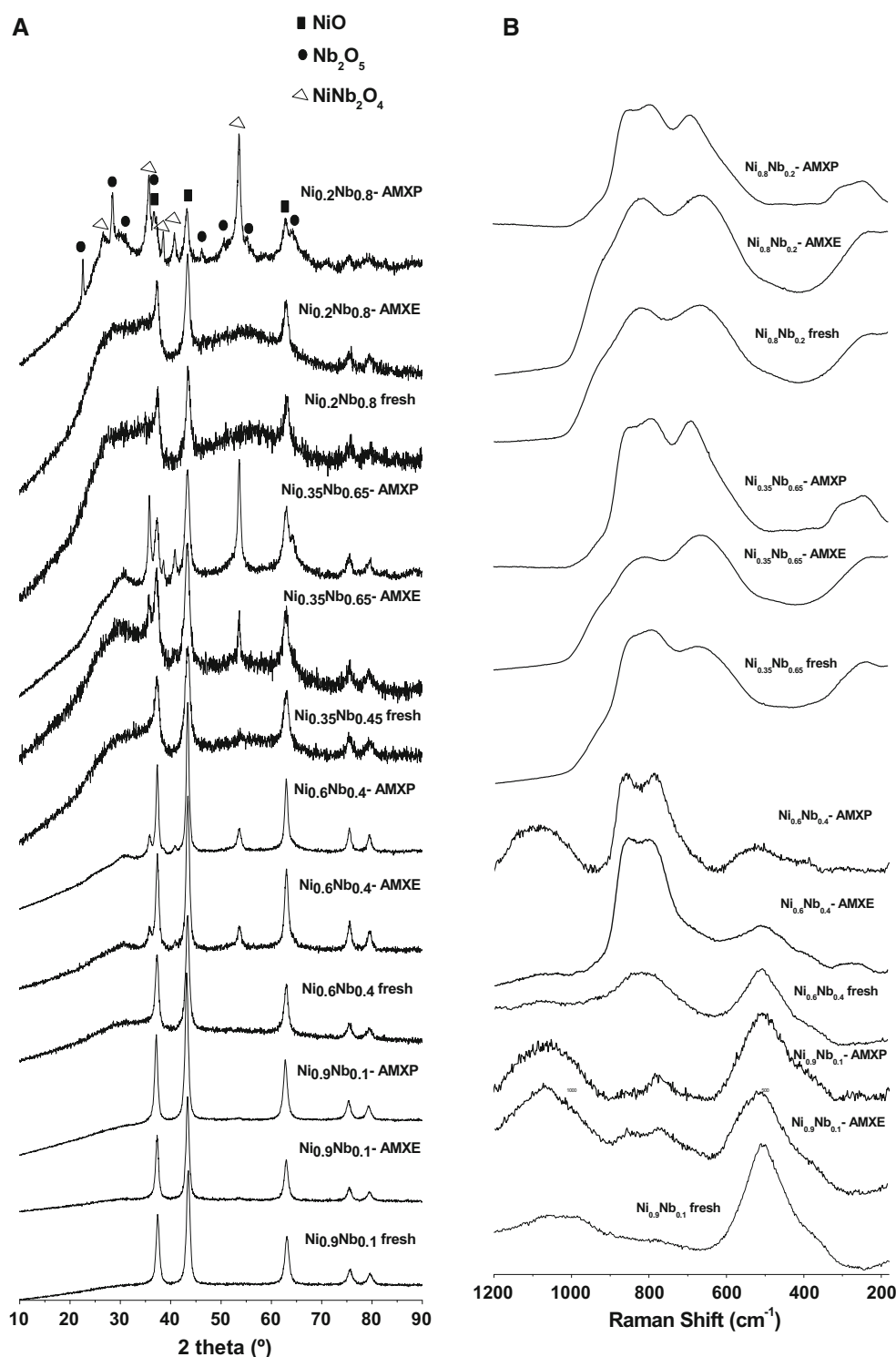
broad Raman band near  $800\text{ cm}^{-1}$ , typical of  $\text{VSbO}_4$ , becomes apparent; this is in line with previous studies that showed how the rutile phase forms during propane ammoxidation [24, 26]. Characterization shows that Sb and V oxide species blend into  $\text{VSbO}_4$  during ethane ammoxidation, in a similar fashion to the trend described elsewhere during propane ammoxidation (Fig. 1a, b). Rutile  $\text{VSbO}_4$  is detected by XRD and Raman spectroscopy in used 1.5Sb1 V/Al AMXe sample. The broad Raman band centered at  $800\text{ cm}^{-1}$  is visible after both propane and ethane ammoxidation reactions (Fig. 1b); spectra show that the structure is not the same after use in ethane or propane reaction. In the case of propane ammoxidation, the amount of  $\text{VO}_x$  species is higher (Raman bands near  $900$  and  $1024\text{ cm}^{-1}$ ); this phase is critical [60] for the reaction mechanism. The transformation of surface  $\text{VO}_x$  into  $\text{VSbO}_4$  implies that surface vanadium (with oxidation state +5) reduces upon incorporation in the rutile lattice, which is composed by since Sb(V) and V(III) ions, as identified by Mössbauer and EPR [61, 62] spectroscopy.

Figure 2 shows the characterization results (XRD patterns and Raman spectra) of the Ni–Nb–O catalytic series. As expected, NiO pattern dominates in the XRD signals of the samples with higher Ni content ( $\text{Ni}_{90}\text{Nb}_{10}$  and  $\text{Ni}_{60}\text{Nb}_{40}$ ). For samples with low Nb contents, XRD patterns of propane used samples ( $\text{Ni}_{20}\text{Nb}_{80}$ -AMXp) show the presence of mixed Nb–Ni–O phases, indicative that has been formed under reaction conditions, this is not detected for the ethane reaction, and occur in a low extension in sample  $\text{Ni}_{20}\text{Nb}_{80}$ -AMXp compared to  $\text{Ni}_{20}\text{Nb}_{80}$ -AMXe. This is

**Fig. 1** XRD patterns (a) and Raman spectra (b) of fresh alumina and fresh 1.5Sb1 V/Al catalyst and used catalysts in both ethane (AMXe) and propane (AMXp) ammoxidation reactions



**Fig. 2** XRD patterns (a) and Raman spectra (b) of fresh and used Ni–Nb–O catalysts in both ethane (AMXe) and propane (AMXp) ammoxidation reactions



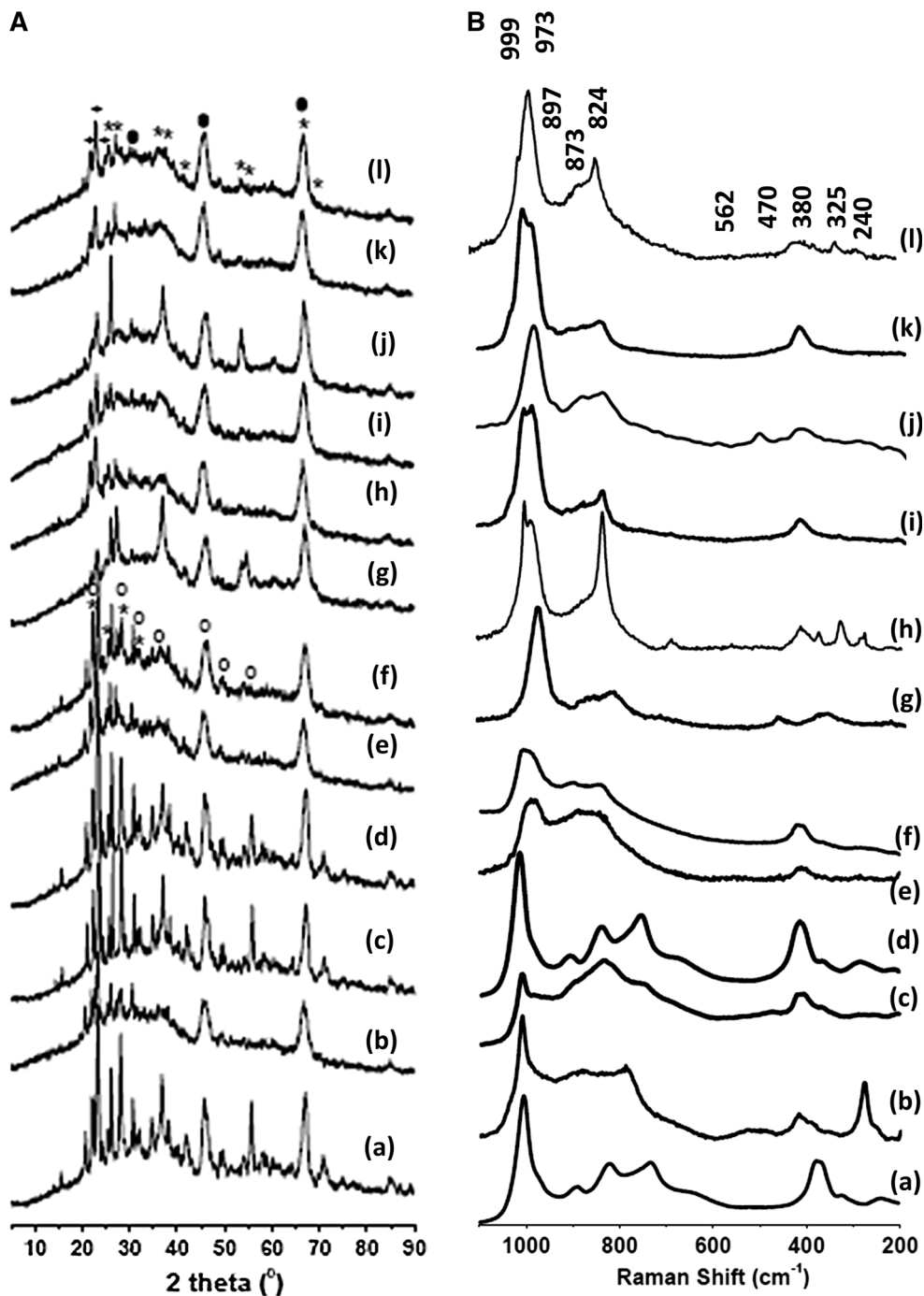
indicative that the formation of Nb–Ni–O mixed phases is more favored in the case of propane ammoxidation than with ethane (both reactions are run at the same temperature, 450 °C). These results are in line with Raman spectra, that shows in the used samples the presence of mixed Nb–Ni–O mixed phases (two Raman bands in the

750–850 cm<sup>-1</sup> range [8, 9]). In the case of Raman spectra, this intensity is similar in the used samples and in some cases these bands are stronger after use. This could be indicative that Nb–Ni–O mixed phases are present in both samples used in ethane and propane reactions, but they are more crystalline in the case of propane reaction (more

intense XRD signals) and the extension of the amorphous Nb–Ni–O mixed phases is higher in the samples used in ethane (stronger Raman bands). In the case of samples with high Nb contents, a more extensive formation of the amorphous Nb–Ni–O mixed phases are detected by Raman spectroscopy (Fig. 2b) in both ethane and propane, although previous work has shown that these mixed phases are Nb-rich and are inactive for the ammoxidation reaction (9).

Figure 3 shows the XRD patterns and Raman spectra of fresh and used Mo–V–Nb–Te–O catalysts. The air-calcined samples exhibit several peaks in the  $22^{\circ}$ – $30^{\circ}$  range, corresponding to mixed Al–Mo–O, Mo–Nb–O and Mo–V–O phases. After reaction these patterns remain visible; and grow stronger if run in propane ammoxidation. In the case of fresh inert-treated samples, there are no Al–Mo–O mixed phases. In this case the rutile and M1 pattern dominates the diffractograms of fresh [55, 56]. After

**Fig. 3** XRD patterns (a) and Raman spectra (b) of fresh and used Mo–V–Nb–Te–O catalysts in both ethane (AMXe) and propane (AMXp) ammoxidation reactions



reaction, Raman bands corresponding to rutile structure tend to disappear, and the bands of M1 phase remain intense.

Raman spectra present a band in the 990–1030  $\text{cm}^{-1}$  range, due to the stretching modes of terminal Mo=O and/or V=O bonds (58). The Mo=O signals appears near 990 whereas the band due to V=O bonds appears near 1020  $\text{cm}^{-1}$ . It must be considered that the Raman section of MoOx species is more intense than that of VOx (58). The signal near 990  $\text{cm}^{-1}$  in the fresh inert-treated sample blueshifts after ethane and propane ammoxidation; this could indicate a higher population of molecularly dispersed vanadium or molybdenum oxide species. This is not observed in the case of samples calcined in air. The Raman band near 380  $\text{cm}^{-1}$ , visible in all the fresh and used samples, belongs to a Mo–V–O phase [56]. The band near 820  $\text{cm}^{-1}$  is characteristic of M1 phase and rutile-type structure [63], and, in line with XRD results, it is more intense in the used samples, especially in those used in propane ammoxidation reaction. The signals near 880–890  $\text{cm}^{-1}$  can be assigned to the stretching modes of Mo–O–M bonds (M=Mo,V) in highly-distorted supported  $\text{Te}_2\text{M}_{20}\text{O}_{57}$  species [64].

Table 2 and Fig. 4 shows ethane conversion and the yield to main products obtained for the ethane ammoxidation reaction at 450 °C. Catalysts belonging to Sb–V–O and Mo–V–Nb–Te catalytic systems are not active, they hardly activate ethane, which conversion is very low; ethylene and acetonitrile are the main products. As expected Ni–Nb–O catalysts are active and selective to acetonitrile formation; the highest acetonitrile yields are obtained for  $\text{Ni}_{0,9}\text{Nb}_{0,1}$  sample. Nb-promoted NiO catalysts are an efficient formulation for the direct ammoxidation of ethane to acetonitrile (7–8). The incorporation of a small amount of niobium into the NiO lattice induces important changes (Ni–Nb–O mixed phase) into the

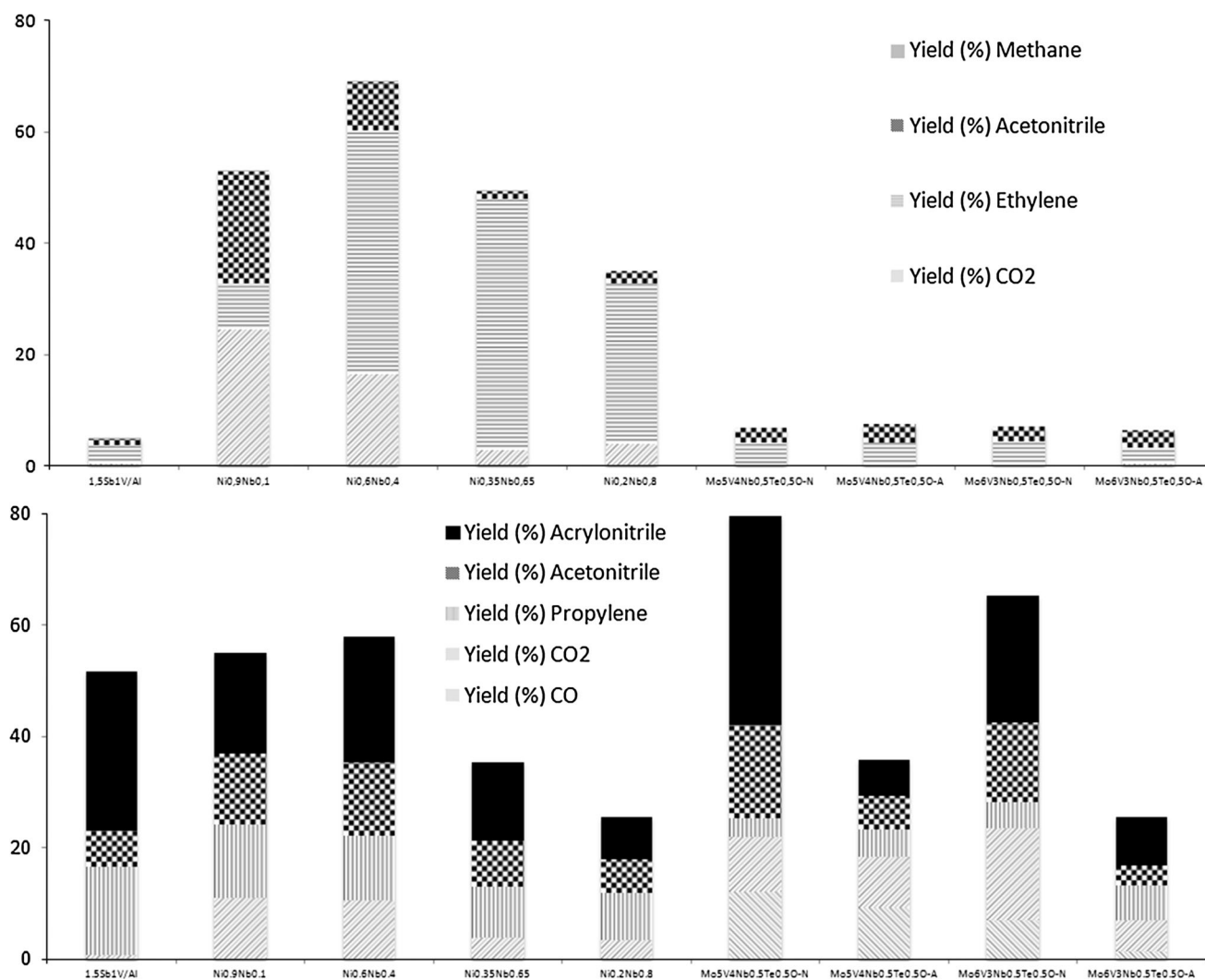
oxide, enhancing the activity and the selectivity for this reaction.

Table 3 and Fig. 4 report propane conversion and the yields to main products at 450 °C. For propane, all catalysts are active. Satisfactory results are obtained with Sb–V–O catalysts (51.8 % propane conversion and 55.4 % acrylonitrile selectivity, 30 % of acrylonitrile yield), these values are consistent with those reported previously (19). As far as we known, the propane ammoxidation reaction has not been evaluated on Ni–Nb–O catalytic system. Data in Table 2 indicate that these materials are also very promising to activate propane, particularly at high Ni content ( $\text{Ni}_{0,9}\text{Nb}_{0,1}$  and  $\text{Ni}_{0,6}\text{Nb}_{0,4}$ ); the selectivity to acrylonitrile is above 30 %. In any case, the acrylonitrile yields obtained are lower than those obtained with Sb–V–O system and also the cracking reaction occurs in a higher extension (a very high selectivity to  $\text{CO}_2$ ). As was described for ethane ammoxidation (8), the best results are obtained for a low amount of niobium, and the activity decreases when increasing the amount of niobium. While Ni–Nb–O materials activate propane (Table 3), ethane conversion (Table 2) is higher. Mo–V–Te catalysts deliver very promising results (Table 3), especially those treated in  $\text{N}_2$  ( $\text{Mo}_5\text{V}_4\text{Nb}_{0,5}\text{Te}_{0,5}\text{O-N}$  and  $\text{Mo}_6\text{V}_3\text{Nb}_{0,5}\text{Te}_{0,5}\text{O-N}$ ). These catalysts contains M1, M2 and rutile phases, which have been reported as active and selective for propane transformation into acrylonitrile and other partial oxidation products, such as acrylic acid (41,56). The best result is afforded by the catalyst with a Mo/V molar ration of 4/4,  $\text{Mo}_5\text{V}_4\text{Nb}_{0,5}\text{Te}_{0,5}\text{O-N}$  (propane conversion of 79.9 % with an acrylonitrile selectivity of 46.8 %, being the acrylonitrile yield of almost 40 %, higher than the data detected for the other catalytic systems studied in present work). Figure 4 suggests that nitrogen insertion is more favorable for propane than ethane in all catalysts. Ethylene is the main product during ethane ammoxidation, while acrylonitrile

**Table 2** Ethane conversion and selectivity to different products for all catalysts on ammoxidation of ethane

Catalyst	Ethane conversion (%)	Selectivity (%)			
		$\text{CO}_2$	Ethylene	Acetonitrile	Methane
1.5Sb1 V/Al	4.9	5.8	67.7	25.9	0.4
$\text{Ni}_{0,9}\text{Nb}_{0,1}$	53.1	46.2	15.5	38.0	0.3
$\text{Ni}_{0,6}\text{Nb}_{0,4}$	69.0	23.8	63.6	12.4	0.2
$\text{Ni}_{0,35}\text{Nb}_{0,65}$	49.3	5.9	91.4	2.5	0.2
$\text{Ni}_{0,2}\text{Nb}_{0,8}$	34.9	11.3	82.7	6.0	0
$\text{Mo}_5\text{V}_4\text{Nb}_{0,5}\text{Te}_{0,5}\text{O-N}$	6.8	0	61.1	38.8	0
$\text{Mo}_5\text{V}_4\text{Nb}_{0,5}\text{Te}_{0,5}\text{O-A}$	7.6	1.7	51.7	46.5	0
$\text{Mo}_6\text{V}_3\text{Nb}_{0,5}\text{Te}_{0,5}\text{O-N}$	7.0	2.4	59.7	37.8	0
$\text{Mo}_6\text{V}_3\text{Nb}_{0,5}\text{Te}_{0,5}\text{O-A}$	6.4	6.5	43.1	50.3	0

Reaction conditions: 200 mg of catalyst, total flow 20  $\text{ml min}^{-1}$ ; feed composition (% volume);  $\text{C}_2\text{H}_6/\text{O}_2/\text{NH}_3/\text{He}$  (9.8/25/8.6/56.5), reaction temperature: 450 °C



**Fig. 4** Yields to main products in both ethane and propane ammoxidation. 200 mg of catalyst, total flow 20 ml min<sup>-1</sup>; feed composition (% volume); C<sub>2</sub>H<sub>6</sub>/O<sub>2</sub>/NH<sub>3</sub>/He (9.8/25/8.6/56.5) or C<sub>3</sub>H<sub>8</sub>/O<sub>2</sub>/NH<sub>3</sub>/He (9.8/25/8.6/56.5), reaction temperature: 450 °C

**Table 3** Propane conversion and selectivity to different products for all catalysts on ammoxidation of propane

Catalyst	Propane conversion (%)	Selectivity (%)					
		CO	CO <sub>2</sub>	Propylene	Acetonitrile	Acrylonitrile	Acetic acid
1.5Sb1 V/Al	51.8	0.2	1.4	30.4	12.4	55.4	0
Ni <sub>0.9</sub> Nb <sub>0.1</sub>	55.2	0	20.1	23.9	22.9	32.9	0
Ni <sub>0.6</sub> Nb <sub>0.4</sub>	58.2	0	18.3	19.8	22.7	38.7	0
Ni <sub>0.35</sub> Nb <sub>0.65</sub>	35.6	0	10.5	26	23.4	39.7	0
Ni <sub>0.2</sub> Nb <sub>0.8</sub>	25.7	0	13.6	32.9	22.8	30.3	0
Mo <sub>5</sub> V <sub>4</sub> Nb <sub>0.5</sub> Te <sub>0.5</sub> O-N	79.9	15.1	12.3	4.2	21.1	46.8	0
Mo <sub>5</sub> V <sub>4</sub> Nb <sub>0.5</sub> Te <sub>0.5</sub> O-A	35.9	25.8	25.5	13.3	16.8	18.3	0
Mo <sub>6</sub> V <sub>3</sub> Nb <sub>0.5</sub> Te <sub>0.5</sub> O-N	65.5	10.7	25.2	7.3	21.7	34.8	0
Mo <sub>6</sub> V <sub>3</sub> Nb <sub>0.5</sub> Te <sub>0.5</sub> O-A	25.6	5.4	22	24	13.9	34.3	0

Reaction conditions: 200 mg of catalyst, total flow 20 ml min<sup>-1</sup>; feed composition (% volume); C<sub>3</sub>H<sub>8</sub>/O<sub>2</sub>/NH<sub>3</sub>/He (9.8/25/8.6/56.5), reaction temperature: 450 °C

and acetonitrile are obtained as main product for all the studied catalysts.

## 4 Discussion

Figures 1, 2 and 3 show that the structures of all catalysts change during reaction. First, in the case of Sb–V–O, Sb and V oxide species blend into rutile VSbO<sub>4</sub> phase, during either propane and ethane ammoxidation. This rutile structure has been described as the active phase during the propane ammoxidation reaction [24, 30]. This is in accordance with activity results (Table 2) that show how this catalyst is active and selective for propane ammoxidation. Conversely, this catalyst does not activate efficiently ethane (Table 1), which conversion remains below 5 %. The mechanism for propane ammoxidation has been described by a combination of theoretical calculations (by density functional theory, DFT) and operando Raman-GC results [65–67]. These results showed the presence of dispersed VOx species is necessary to first activate propane into propylene; then, the rutile absorbs ammonia and propylene at nearby V and Sb sites, respectively yielding acrylonitrile. VOx species are able to activate both propane and ethane molecules, since supported VOx catalysts are well known as active for both ethane and propane dehydrogenation reactions [68, 69]. The theoretical data indicated (65) that the adsorption of ethane and ethylene on VSbO<sub>4</sub> rutile sites cannot compete with that of ammonia, thus inhibiting the reaction. There is some conversion, which must be related to the presence of dispersed vanadium species, not integrated into VSbO<sub>4</sub>. Despite marginal activity, reaction conditions do rearrange vanadium and antimony oxide species into the VSbO<sub>4</sub> rutile structure in this catalyst. The extent of the formation is this phase during ethane ammoxidation is significantly lower than that during propane ammoxidation, though. This would be indicative of a much lower ammoxidation turnover. The M1 and Mo–V–O rutile active phases in Mo–V–O are another example of structures capable of activating propane ammoxidation (Table 2; Fig. 4), whereas they are much less efficient for ethane conversion, which does not reach 10 % (Table 1).

The Ni–Nb–O catalytic system activates both ethane and propane ammoxidation. In this case some rearrangement of the structure of catalysts is also apparent after reaction. Conversely to Sb–V–O and Mo–V–O systems, both ethane and propane are converted to similar extents on Ni–Nb–O system. In both cases, the most active catalysts are those with lower Nb content (Ni<sub>0.9</sub>Nb<sub>0.1</sub> and Ni<sub>0.6</sub>Nb<sub>0.4</sub>), with alkane conversion around 50–60 % and nitrile selectivity near 32–38 % (Table 1 and 2). Ni–Nb–O system does activate the methyl group in ethane, whereas V–Sb–O and

Mo–V–Nb–Te–O systems are not capable of activating the methyl group, and subsequently to transform ethane into its nitrile. This ability of Ni–Nb–O to activate ethane and propane must be related with its particle size and also to the reaction mechanism. In the case of Sb–V–O and Mo–V–O catalytic systems, the reaction occurs via two active sites, first, the alkane is dehydrogenated (most probably in VOx dispersed sites) into propylene, and then the nitrogen insertion occurs in the rutile structure [65–67], this mechanism would facilitate N-insertion, since the results showed in Fig. 4 clearly show how the amount of acetonitrile and acrylonitrile is higher in the case of propane ammoxidation. In the case of ethane reaction, it seems that only one site is involved (Nb-promoted NiO site), being the dehydrogenation the most favorable route (high selectivity to ethylene, as it is shown in Fig. 4). In this case the N-insertion in order to form acetonitrile can occur in the adsorbed ethylene or in the gas phase.

## 5 Conclusions

V–Sb–O, Mo–V–Nb–Te–O and Ni–Nb–O catalytic systems exhibit distinct behaviors during ethane and propane ammoxidation. V–Sb–O and Mo–V–Nb–Te–O are efficient for propane activation but they're hardly efficient for ethane activation. The discrete ethane ammoxidation activity might be related to molecularly dispersed vanadium species that would convert ethane into its olefin. On the contrary, all these catalysts are efficient for propane ammoxidation, in this case previous studies show that the reaction mechanism may occur with the concurrence of two sites (molecularly dispersed VOx interacting with VSbO<sub>4</sub> rutile phase in the latter, and via M1/rutile and M2 phase interaction in the latter). Under ammoxidation conditions, they would first dehydrogenate propane into propylene (either on dispersed VOx or on M1/rutile) and then propylene would react into its nitrile on the VSbO<sub>4</sub> and M2 phase, respectively. Ethane (with two methyl groups) and ethylene (with two methylene groups) are not efficiently activated by VSbO<sub>4</sub> or Mo–V–Nb–Te–O phases.

The NiO-based catalyst is totally different. It crystallizes with cubic rock salt structure and it becomes more active when the structure is distorted with a small amount of Nb, which forms a mixed Nb–Ni–O phase. Such structure is able to activate the methyl groups and subsequently the ethane molecule as well as propane can be adsorbed. In this case the reaction mechanism seems to occur in only one step, being the dehydrogenation step to form ethylene the most favorable route.

**Acknowledgments** The Ministry of Science and Innovation (Spain) funded this study under project (CTQ2014-57578-R). Ricardo López-

Medina thanks Spanish AECID for a PhD fellowship and Elizabeth Rojas thanks CONACYT for a PhD program fellowship.

## References

- Martin A, Narayana V (2010) *ChemCatChem* 2:1504–1522
- Guerrero-Pérez MO, Bañares MA (2015) *Catal Today* 239:25–30
- Chemical Week, February 14 (2013). <http://www.chemweek.com/archives/home/?skp=7940>
- Heracleous E, Lemonidou AA (2010) *J Catal* 270:67
- Heracleous E, Lemonidou AA (2006) *J Catal* 237:162
- Rojas E, Guerrero-Pérez MO, Bañares MA (2009) *Catal Commun* 10:1555–1557
- Rubio-Marcos F, Rojas E, López-Medina R, Guerrero-Pérez MO, Bañares MA, Fernandez JF (2011) *ChemCatChem* 3:1637–1645
- Rojas E, Guerrero-Pérez MO, Bañares MA (2013) *Catal Lett* 143
- Rojas E, Delgado JJ, Guerrero-Pérez MO, Bañares MA (2013) *Catal Sci Technol* 3:3173
- Guerrero-Pérez MO, Rojas E, Gutiérrez-Alejandre A, Ramírez J, Sánchez-Minero F, Fernández-Vargas C, Bañares MA (2011) *PCCP* 13(20):9260–9267
- Catani R, Centi G, Trifiro F, Grasselli RK (1992) *Ind Eng Chem Res* 31:107–119
- Grasselli RK (1999) *Catal Today* 49(1–3):141–153
- Grasselli RK (2002) *Top Catal* 21:79–88
- Li KT, Shyu NS (1997) *Ind Eng Chem Res* 36:1480
- Zhang H, Zhang J, Sun K, Feng Z, Ying P, Li C (2006) *Catal Lett* 106:89–93
- Guerrero-Pérez MO, Janas J, Machej T, Haber J, Lewandowska AE, Fierro JLG, Bañares MA (2007) *Appl Catal B* 71(1–2):85–93
- Shishido T, Inoue A, Konishi T, Matsuura I, Takehira K (2000) *Catal Lett* 68:215
- Andersson A, Andersson SLT, Centi G, Grasselli RK, Sanati M, Trifiro F (1994) *Appl Catal A* 113:43–57
- Guerrero-Pérez MO, Fierro JLG, Vicente MA, Bañares MA (2002) *J Catal* 206:339–348
- Guerrero-Pérez MO, Rivas-Cortés JL, Delgado Oyagüe JA, Fierro JLG, Bañares MA (2008) *Catal Today* 139:202–208
- Guerrero-Pérez MO, Bañares MA (2008) *ChemSusChem* 1(6):511–513
- Calvino-Casilda V, Guerrero-Pérez MO, Bañares MA (2009) *Green Chem* 11:939–941
- Calvino-Casilda V, Guerrero-Pérez MO, Bañares MA (2010) *Appl Catal B* 95(3–4):192–196
- Guerrero-Pérez MO, Bañares MA (2002) *Chem Commun* 12:1292–1293
- Guerrero-Pérez MO, Kim T, Bañares MA, Wachs IE (2008) *J Phys Chem C* 112:16858–16863
- Guerrero-Pérez MO, Bañares MA (2007) *J Phys Chem C* 111:1315–1322
- Centi G, Marchi F, Perathoner S (1997) *Appl Catal A* 149:225
- Landa-Cánovas AR, García-García F, Hansen S (2010) *Catal Today* 158:156
- Landa-Cánovas AR, Nilsson J, Hansen J, Stahl K, Andersson A (1995) *J Solid State Chem* 116:377
- Guerrero-Pérez MO, Bañares MA (2004) *Catal Today* 96:265
- Kim YC, Ueda W, Moro-oka Y (1992) *Catal Today* 13:673
- Sureh DD, Orloff DA, Brazdil JF, Glaeser LC, Friendlich MS (1988) US Patent 47060159
- Glaeser LC, Brzdil JF, Toft MA (1988) US Patents 4843655, 4835125, 4837192
- Kim JS, Woo SI (1994) *Appl Catal* 110:207
- Ushikubo T, Oshima K, Kayou A, Vaarkamp M, Hatano M (1997) *J Catal* 169:394
- Grasselli RK, Trifiro F (2011) *Top Catal* 54:587
- Grasselli RK, Goddard WA (2008) *Top Catal* 50:1
- Yuan L, Guliants VV (2009) *J Porous Mat* 16:613–622
- Carreon MA, Guliants VV, Guerrero-Perez MO, Bañares MA (2009) *Catal Commun* 4:416–420
- Muthukumar K, Yu J, Xu Y, Guliants VV (2011) *Top Catal* 54:605–613
- López-Medina R, Rojas E, Bañares MA, Guerrero-Pérez MO (2012) *Catal Today* 192:67–71
- Yuan L, Guliants VV (2009) *J Porous Mater* 16:613–622
- Korovchenko P, Shiju NR, Dozier AK, Graham UM, Guerrero-Pérez MO, Guliants VV (2008) *Top Catal* 50:43–51
- Grasselli RK (2005) *Catal Today* 99:23–31
- Celaya Sanfiz A, Hansen TW, Teschner D, Schnörch P, Girgsdies F, Trunschke A, Schlögl R, Hong Looi M, Abd Hamid SBJ (2010). *Phys Chem C* 114: 1912–1921
- Pyrz WD, Blom DA, Sadakane M, Kodato K, Ueda W, Vogt T, Buttrey DJ, Natl P (2010) *Acad Sci USA* 107:6152–6157
- Pyrz WD, Blom DA, Sadakane M, Kodato K, Ueda W, Vogt T, Buttrey DJ (2010) *Chem Mater* 22:2033–2040
- Botella P, García-González E, López-Nieto JM, González-Calbet JM (2005) *Solid State Sci* 7:507–519
- Holmberg J, Grasselli RK, Andersson A (2004) *Appl Catal A* 270:121–134
- Baca M, Aouine M, Dubois JL, Millet JMM (2005) *J Catal* 233:234–241
- De Santo Jr P, Buttrey DJ, Grasselli RK, Lugmair CG, Volpe AF Jr, Toby BH, Vogt T (2004) *Keitschrift fur Kristallographie* 239(3):152–165
- Hansen S, Stahl K, Nilsson R, Andersson A (1993) *J Solid State Chem* 102:340
- Guerrero-Pérez MO, Fierro JLG, Bañares MA (2003) *Catal Today* 78(2003):387–396
- Guerrero-Pérez MO, Fierro JLG, Bañares MA (2006) *Top Catal* 41:43–53
- López-Medina R, Golinska H, Ziolk M, Guerrero-Pérez MO, Bañares MA (2010) *Catal Today* 158(1–2):139–145
- López-Medina R, Fierro JLG, Guerrero-Pérez MO, Bañares MA (2010) *Appl Catal A* 375:139–145
- López-Medina R, Rojas E, Bañares MA, Guerrero-Pérez MO (2012) *Catal Today* 192:67–71
- Bañares MA, Wachs IE (2002) *J Raman Spectrosc* 33:359
- Guerrero-Pérez MO, Fierro JLG, Bañares MA (2006) *Catal Today* 118:366–372
- Guerrero-Perez MO, Bañares MA (2007) *J Phys Chem C* 111:1315–1322
- Birchall T, Sleight AW (1976) *Inorg Chem* 15:868
- Berry FJ, Brett ME (1983) *Inorg Chim Acta* 7:L205
- Li X, Buttrey DJ, Blom DA, Vogt T (2011) *Top Catal* 54:614–626
- Botella P, García-González E, López JM (2005) *Solid State Sci* 7:507
- Rojas E, Calatayud M, Bañares MA, Guerrero-Perez MO (2012) *J Phys Chem C* 116:9132–9141
- Rojas E, Calatayud M, Guerrero-Perez MO, Bañares MA (2010) *Catal Today* 158:178–185
- Rojas E, Calatayud M, Guerrero-Perez MO, Bañares MA (2012) *Catal Today* 187:212–213
- Cavani F, Ballarini N, Cericola A (2007) *Catal Today* 127:113–131
- Bañares MA (1999) *Catal Today* 51:319–348